Vol. 5 • No. 10 • May 25 • 2016

www.advhealthmat.de

ADVANCED HEALTHCARE MATERIALS

WILEY-VCH

ADVANCED HEALTHCARE MATERIALS
www.advhealthmat.de

Diamond-Nanoneedle-Array-Facilitated Intracellular Delivery and the Potential Influence on Cell Physiology

Xiaoyue Zhu, Muk Fung Yuen, Li Yan, Zhenyu Zhang, Fujin Ai, Yang Yang, Peter K. N. Yu, Guangyu Zhu, Wenjun Zhang,* and Xianfeng Chen**

Vertical arrays of nanostructures can provide access to the cell cytoplasma and probe intracellular molecules. Here, the simple combination of diamond nanoneedle arrays with centrifugation-induced supergravity is shown to efficiently deliver drugs and biomaterials into the cytosol within several minutes, negotiating the endocytososomal system. The potential influence of the technique on cell metabolism is thoroughly studied. By detecting the phosphorylated histone variant H2AX (pH2AX) in the nucleus, it is proved that the operating process will not lead to DNA double-strand breaks. However, the mechanical disruption can temporarily improve the permeability of the cell membranes. Nanoneedle treatment affects cell metabolism at multiple points. The treatment can slightly elevate the apoptotic signal in A549 cells and can significantly increase the production of reactive oxygen species (ROS) in cells, particularly if combined with anticancer drugs. Meanwhile, the activity of cytosolic glucose 6-phosphate dehydrogenase (G6PD) is also raised to counterbalance the elevated ROS content. A detected depolarization of the mitochondrial membrane potential suggests mitochondrial involvement in the intracellular redox reactions and cell apoptosis which are induced by diamond nanoneedle treatment. Overall this study provides a novel understanding on the intracellular delivery mediated by nanoneedles, especially the impact on cell physiology.

1. Introduction

Delivery of biological molecules and fluorescent probes into living cells and tissues is of great importance.[1,2] A broad range of cationic polymers, lipids, transfection, and complex-assembling reagents, as well as nanomaterials have been widely used in cytosolic delivery.[3–11] However, many factors affect the efficiency of cargo molecules delivery, such as cell type, cell number, media, carrier-relating cytotoxicity, and low transfection efficacy for hard transfecting cells.[12,13] Recently, as a physical approach, vertical nanostructure arrays are reported to conveniently facilitate intracellular delivery with high throughput.[14] For example, vertical silicon nanowires have been developed as a universal platform for transporting a range of cargos into living cells, including DNAs, RNAs, peptides, and proteins.[3,15] In the delivering process, cells are cultured on the vertical nanostructures for a period of time so that the nanowires spontaneously penetrate cell's membranes and the precoated biomolecules on the nanostructures can be slowly released into the cells. Similarly, aluminum oxide nanostraws have also been applied to deliver cargos into cells but the difference is that the nanostraws are hollow and integrated with a reservoir so materials can be directly injected to cells once the nanostraws pierce into cells during the culturing.[16] The advantage of these methods is that biomolecules can be transported into cells without the requirement of chemical modification or viral packaging. However, some cell functions might be perturbed by culturing on such nanostructures for an extended period of time. For example, it has been discovered that HeLa cells grow slowly[17] and temporarily develop irregular contours when culturing on silicon nanowires and the penetration of nanowires into cells leads to lipid scrambling although this can be reversed in healthy cells.[15] In addition, Persson et al. explored that fibroblasts cultured on similar nanostructures display impaired cell division, increased reactive oxygen species (ROS) content and ultimately DNA damage.[18] Liu et al. found that mesenchymal stem cells exhibit significantly different adhesion, proliferation and differentiation behavior when compared to those on flat substrates.[19]

X. Zhu, M. F. Yuen, Dr. L. Yan, Z. Zhang, Dr. Y. Yang, Prof. W. Zhang
Center of Super-Diamond and Advanced Films (COSDAF) and Department of Physics and Materials Science
City University of Hong Kong
Hong Kong SAR
E-mail: apwjzh@cityu.edu.hk
F. Ai, Prof. G. Zhu
Department of Biology and Chemistry
City University of Hong Kong
Hong Kong SAR
E-mail: guangzhu@cityu.edu.hk
Prof. P. K. N. Yu
Department of Physics and Materials Science
City University of Hong Kong
Hong Kong SAR
Dr. X. Chen
School of Chemistry and Forensic Sciences
Faculty of Life Sciences
University of Bradford
United Kingdom, BD7 1DP
E-mail: xianfeng_chen@hotmail.com

DOI: 10.1002/adhm.201500990

To alleviate these problems, we developed diamond nanoneedle arrays for enhanced intracellular delivery.[20–22] In our approach, instead of culturing cells on the vertical nanostructures for spontaneous penetration over a period, we allow the nanoneedles to actively disrupt the cell membranes within a very short duration (e.g., seconds to minutes) by a precisely controlled centrifugation force or applying a cell suspension to the nanostructures with a certain speed.[20–22] This platform has been demonstrated capable of effectively delivering fluorescent cell probes (iridium(III) polypyridine complex, FITC–dextran, propidium iodide (PI), and calcein AM, semiconductor quantum dots), drug molecules (cisplatin), and genes (siRNA and DNA) to various cell lines.[20,21,23] Very recently, with a similar manner, carbon nanosyringe arrays have also been employed to facilitate the delivery of bioactive molecules to hard-to-transfect cells.[24] Beyond these in vitro uses on cell lines, biodegradable silicon nanoneedles with 50 nm diameter tips are applied in vivo to transfect VEGF-165 gene and induce sustained neovascularization.[25] This work sets a new milestone in the application of nanoneedle arrays for delivering biological functional molecules to the cells in living tissues.

Despite the promising future of this new approach, the effect of the method on cell physiology has not been investigated although it is of great importance to the design of the nanostructures and operation parameters. In this study, we apply cells in a suspension to diamond nanoneedle arrays with centrifugation force for efficient intracellular delivery and then investigate the potential influence of the method on cell's DNA, ROS content, mitochondrial membrane potential and glucose-6-phosphate dehydrogenase (G6PD) activity. These findings will certainly improve our understanding of the technology of using this type of vertical nanostructures for intracellular delivery and should provide guidance to better design the platform for practical applications.

2. Results and Discussion

2.1. Fabrication of Diamond Nanoneedle Arrays

Diamond nanoneedle arrays were fabricated by forming a polycrystalline diamond thin film first on silicon substrates followed by microwave plasma etching. We specifically chose diamond to manufacture nanoneedle arrays because of its outstanding mechanical strength and inertness. Two representative SEM images of diamond nanoneedle arrays are shown in **Figure 1**a. These nanoneedles are conical in shape with a height of 2 μm and a density of 1×10^6 mm^{-2}. The tip of diamond nanoneedle arrays is about 50 nm.

2.2. Diamond Nanoneedle Arrays to Facilitate Intracellular Delivery

In our previous reports,[20,22] we used diamond nanoneedle arrays to improve intracellular delivery by applying a cell suspension to the nanostructures with a certain speed. The

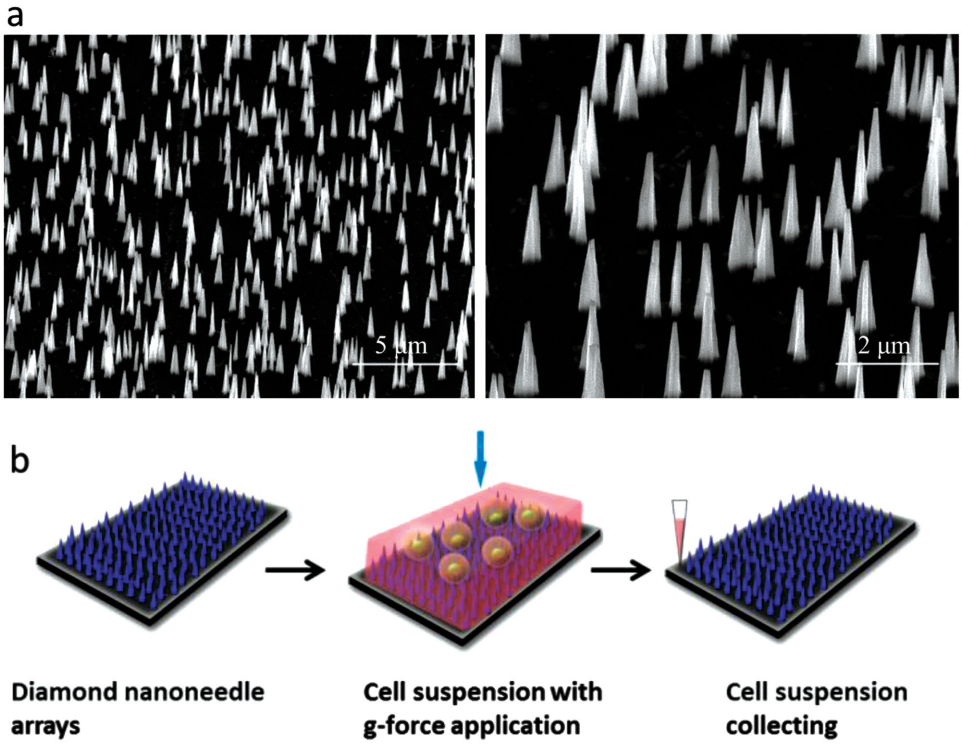

Figure 1. a) SEM images of diamond nanoneedle arrays. The scale bars indicate 5 (left) and 2 μm (right). b) Schematic representation of diamond nanoneedle-mediated intracellular delivery with centrifugal g-force application. A cell suspension is applied to the surface of a diamond nanoneedle array and then a centrifugation force is used to control the disruption of the cell membranes for facilitated intracellular delivery. At the end of the process, the cell suspension is collected.

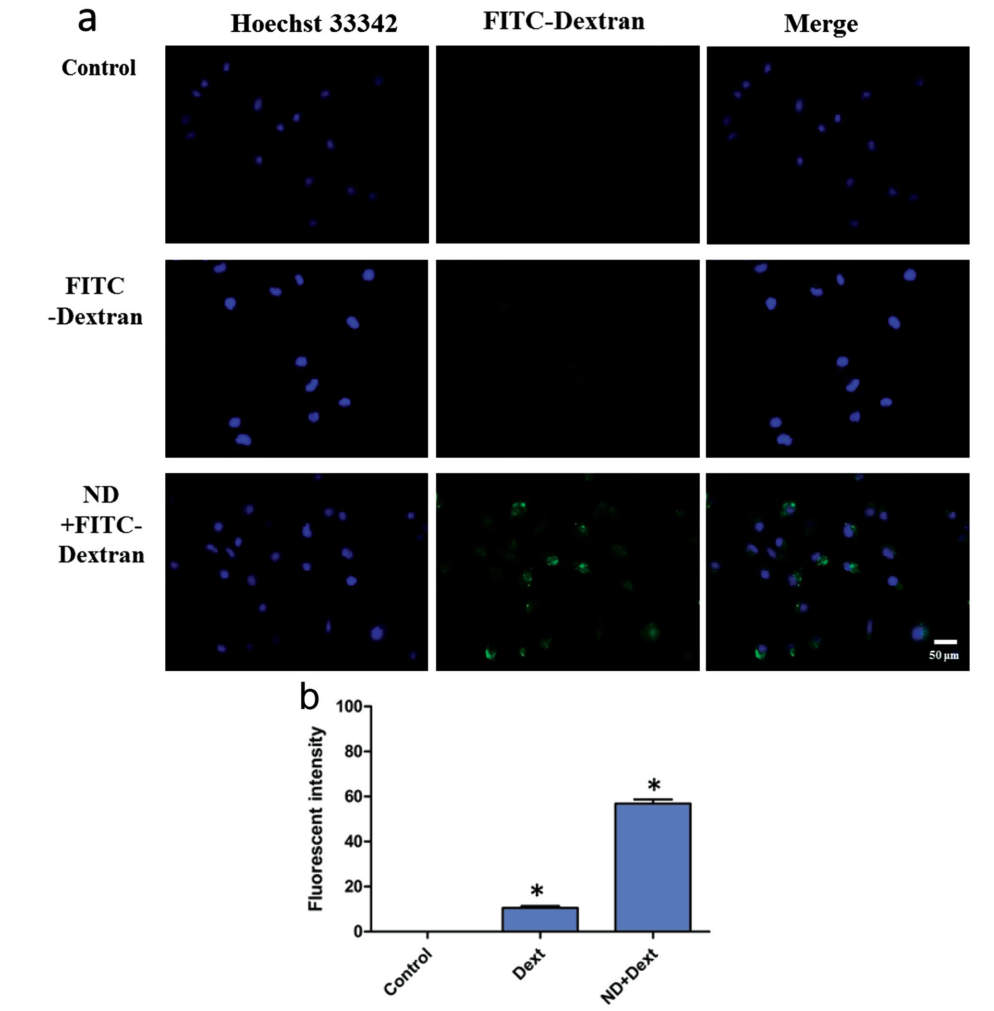

method is high-throughput and effective but lack of precise control. To further improve this approach, herein, we apply a cell suspension on a diamond nanoneedle arrays and then apply centrifugation force to carefully control the interaction between cells and nanostructures for enhanced intracellular delivery (Figure 1b). At the end of the process, the cell suspension is collected.

Before measuring the potential influence of the technology on cell physiology, we firstly proved that this system could be used to rapidly transport fluorescent molecules into cells. In our experiment, we chose FITC-labeled dextran with large molecular weight of 10 000 Da for this evaluation and the results are presented in **Figure 2**a. Three groups were performed including untreated cells, cells incubated with FITC–dextran without nanoneedles treatment, and cells treated with both nanoneedles and FITC–dextran. From the figures, it can be observed that the untreated cells and the cells incubated with FITC–dextran for 30 minutes but without nanoneedles treatment display no or negligible fluorescence. In great contrast, FITC–dextran is able to quickly transport into the nanoneedles treated A549 cells within only 5 min. Calculated by the software Image J, the relative fluorescence intensities in the cells without and with diamond nanoneedle application are 10% and 57%, respectively (Figure 2b).

After confirming that the method can effectively deliver fluorescent molecules into cells, we then investigated whether this method was capable of improving the delivery of biologically functional small molecules to cells. Tests on three groups were conducted. In one group, 0.2 μg mL^{-1} of cisplatin was added into cell suspension and then the cells were placed on a diamond nanoneedle substrate followed by application of centrifugation force of 30 s only. Following that, the treated cells were cultured for 48 h for viability measurement. Another group was A549 cells in a suspension containing the same concentration of cisplatin but without nanoneedle treatment. Untreated A549 cells were used as negative control group. The cell viability of all three groups was measured 48 h later. The results were normalized to the number of cells in the negative control group. Compared with the negative control group, there was no reduction of cell viability observed in the group of cells treated with cisplatin but without nanoneedle treatment. It indicates that the concentration of cisplatin is very low and not enough to kill cells. However, with additional nanoneedle treatment, the viability of cells dramatically drops by 32% in the presence of the same concentration of cisplatin (Figure 2c). Considering that the duration of nanoneedle treatment time might affect the drug delivery efficiency, we tested the cell viability by increasing the centrifugation time from 30 s to 5 min. As shown in Figure 2d, the viability of cells decreases over 60%. Overall, the results in Figure 2 demonstrate that this method is efficient in intracellular delivery.

Since the nanoneedle platform has been proved to be an efficient system in cytosolic delivery, we also expect that diamond nanoneedle arrays can enhance the delivery of drugs into drug resistant cells. We tested the potential efficiency of this system in doxorubicin resistant MCF7 cell line (MCF7/ADR) by flow cytometry. Three groups were conducted in the experiment. The first group of untreated MCF7/ADR cells was used as a negative control group. The second group of MCF7/ADR cells was incubated with 2 μg mL^{-1} doxorubicin for 5 min. The third group of cells was treated with both nanoneedles and doxorubicin at the same time. The results are described in Figure 2e. It can be seen that the efficiency of MCF7/ADR doxorubicin delivery in the diamond nanoneedle arrays group (27.53) is higher than that in the doxorubicin free-delivery group (17.11). The fluorescent intensity of doxorubicin in the control group is only 5.6. Furthermore, we also evaluated the use of nanoneedle treatment in helping doxorubicin to kill MCF7/ADR cells. When MCF7 cells are cultured with 1 μg mL^{-1} doxorubicin for 48 h, the cell viability is only about 10% (Figure S1, Supporting Information). In comparison, for MCF7/ADR cells, this dose is even not strong enough to induce significant cell death. Attractively, with the aid of diamond nanoneedle arrays treatment, the viability of MCF7/ADR cells can be reduced to about 50% (Figure 2f) in the presence of the same concentration of doxorubicin. Collectively, these results suggest that diamond nanoneedle arrays be an efficient delivering platform even for drug resistant cells.

2.3. Toxicity of Diamond Nanoneedle Array Treatment

While confirming that diamond nanoneedle treatment is able to facilitate the transport of molecules into cells and improve the efficacy of drugs, the next key question is whether the methodology leads to cytotoxicity.

To investigate if our intracellular delivery approach has any impact on cell proliferating ability, we firstly performed a viability study of cells. One group of untreated cells was used as a control group. The other group of cells was treated with diamond nanoneedle arrays by centrifugation at 120 g for 5 min at room temperature. The total number of cells at the beginning of the experiments in each group is about 30 000. Then the cell viabilities of both groups of cells were determined with an

Figure 2. Cytosolic delivery by diamond nanoneedle arrays. a) Fluorescence images of A549 cells after delivery of FITC–dextran (10 000 MW) under different conditions (no treatment, incubation with FITC-dextran, incubation with FITC–dextran and diamond nanoneedle treatment). Hoechst 33342 was used to stain the nucleic acid. Green signal indicates the fluorescence of FITC–dextran. b) Quantification of fluorescent intensity within the cells by using Image J. c,d) Cell viability of A549 cells under different conditions (no treatment, incubation with 0.2 μg mL^{-1} cisplatin (cisplatin-CT), treated with diamond nanoneedle arrays (ND) and incubation with 0.2 μg mL^{-1} cisplatin. MTT assays were conducted at 48 h after incubation. c) Nanoneedle arrays treatment of cells for 30 s. d) Nanoneedle arrays treatment of cells for 5 min. (*$p < 0.01$). e) The delivery of doxorubicin to MCF7/ADR cells with and without nanoneedle treatment. Flow cytometry analysis of the fluorescence intensities of doxorubicin was tested immediately after drug delivery. f) Cell viabilities of MCF7/ADR cells treated with 1 μg mL^{-1} doxorubicin with the aid of diamond nanoneedles (Doxorubicin-ND) or without using nanoneedles (Doxorubicin-CT). Untreated MCF7/ADR cells were used as negative control. (*$p < 0.01$; NS: nonsignificant).

MTT assay and the results are shown in **Figure 3**a. It is clear that the diamond nanoneedle arrays treatment does not cause measurable cell death in comparison with the untreated cells.

Following cytotoxicity measurement, to find out whether our approach induces DNA damage, we investigated the integrity of genomic DNA in cells. One response to double-strand DNA break is the need of phosphorylated histone variant H2AX (pH2AX) in the recruitment of proteins responsible for DNA repairing.[26,27] In other words, the pH2AX indicates DNA double-strand breaks. Therefore, we measured the level of DNA damage by specific antibody-based detection of pH2AX in nucleus. In the test, cells were treated by diamond nanoneedle arrays followed by culturing in a 96-well plate for 3, 6, and 24 h. Untreated cells were again used as a negative control group. Then all of the groups of cells with different culturing times were labeled with pH2AX mouse monoclonal antibody. Subsequently, a fluorescent secondary antibody was used to bind to the primary pH2AX antibody and the fluorescence intensities were determined for quantity analysis of pH2AX. As shown in Figure 3b, the amount of pH2AX does not have significant difference between the control group and the group treated by nanoneedle arrays at all three different time points. This indicates that the diamond nanoneedle array treatment does not lead to DNA double-strand breaks.

Besides genotoxicity, we also measured the integrity of cytoplasm membrane at 3, 6, and 24 h after diamond nanoneedle array treatment with the image-iT dead green viability stain. We previously demonstrated that diamond nanoneedle disruption to cells can lead to the permeation of ethidium homodimer-1 (EthD-1) through the cell membranes.[21] EthD-1 is a high-affinity nucleic acid stain that is weakly fluorescent until bound to DNA and emits red fluorescence. In the test, EthD-1 was applied when cells were undergoing nanoneedle treatment. However, here, we add Image-iT dead green at 3, 6, and 24 h after nanoneedle treatment. Image-iT dead green staining is a microscopy-based fluorescent assay for dead cells. It is impermeable to health cells but become permeant when the cytoplasm membrane is compromised. The result about image-iT dead green staining is presented in Figure 3c. It is clear that there is negligible difference in fluorescence intensity between the untreated cells and the group treated by nanoneedle arrays at different time points, suggesting that the cell membranes recover their integrity soon after nanoneedle disruption (Figure 3c).

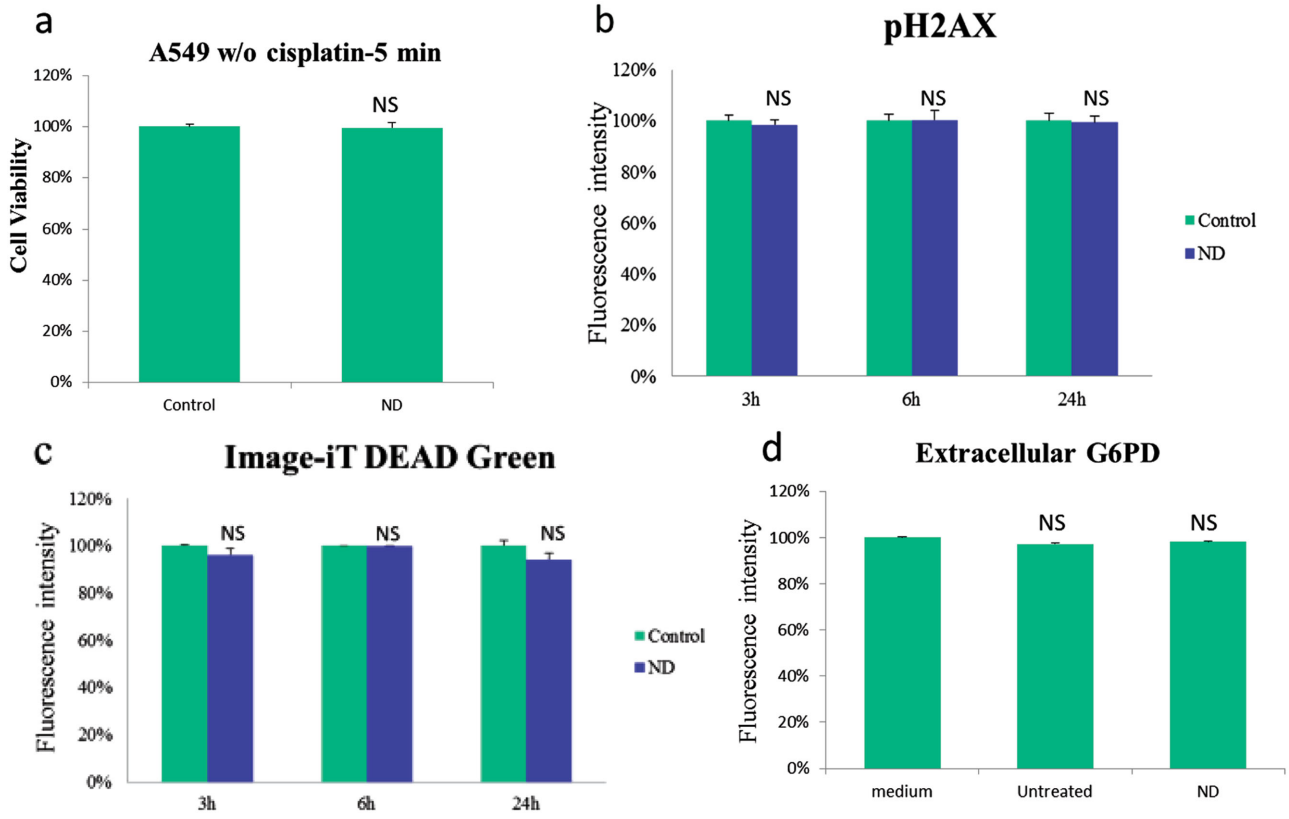

Figure 3. a) Viability of A549 cells treated with diamond nanoneedle arrays. Cell viability was detected by MTT assay. Untreated cells were used as a control group. b) Genotoxicity assay and c) cell membrane integrity analysis. After being treated by diamond nanoneedle arrays, A549 cells were cultured in a 96-well plate for 3, 6, or 24 h. DNA double-strand breaks were investigated by monoantibody pH2AX detection. The fluorescence intensity of pH2AX signal was detected by using a TRITC filter (E_X/E_M 555/565 nm). The integrity of plasma membrane was evaluated by image-iT DEAD green viability staining. The fluorescence intensity was assessed by a FITC filter (E_X/E_M 488/515 nm). d) Detection of extracellular G6PD level in A549 cells treated with a nanoneedle array. A549 cells were treated with a nanoneedle array (ND) followed by culturing of 24 h, and then the extracellular G6PD release was measured (E_X/E_M 530/590 nm). Cell culture medium alone and untreated cells were used as control groups. (*$p < 0.01$; NS: non-significant)

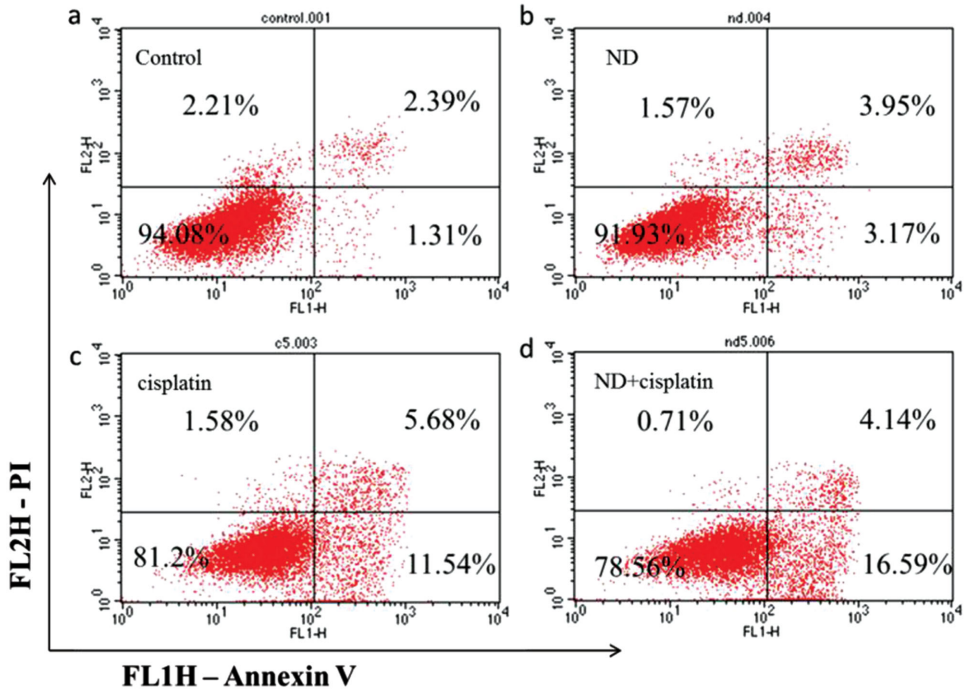

Figure 4. Flow cytometry analysis of apoptosis and necrosis of A549 cells. a) Untreated cells; b) Cells treated with a diamond nanoneedle array alone; c) Cells incubated with 5 μg mL^{-1} of cisplatin for 24 h. d) Cisplatin was added to a cell suspension with a concentration of 5 μg mL^{-1} and the suspension was applied to a diamond nanoneedle array for treatment for 5 min. Subsequently, the cell suspension was collected and cultured in a 96-well plate for 24 h. The analysis was conducted after 24 h incubation. For all groups, A549 cells were stained and analyzed by 488 nm excitation with 530/30 nm and 575/24 nm bandpass filters and collected by means of a standard 100 μL min^{-1} collection rate. Early apoptotic cells are shown in the lower right quadrant, and necrotic cells are shown in the upper left quadrant.

We next monitored the release of glucose 6-phosphate dehydrogenase (G6PD) from treated cells into the surrounding medium. G6PD is a cytosolic enzyme and can leak from dead cells. The released amount of G6PD in cell medium correlates with the number of dead cells in the sample. Since the level of G6PD activity in common cell culture sera is much lower than many other enzymes, such as lactate dehydrogenase, this assay can be more precise and effective. A549 cells were treated with a diamond nanoneedle arrays following by 24 h culturing in a 96-well plate. The extracellular G6PD level was detected by following the vibrant cytotoxicity assay kit. The mechanism is to oxidize glucose 6-phosphate by G6PD and generate NADPH, which causes the reduction of resazurin (a blue dye) to yield fluorescent resorufin for measurement. Cell culture medium and untreated cells were used as two control groups. The result shows that there is no significant difference among these three groups in the amount of extracellular G6PD (Figure 3d). These findings suggest that diamond nanoneedle treatment delivering system does not affect the viability of the cells. This is in line with the result shown in Figure 3a.

2.4. Nanoneedle Treatment Leads to Apoptosis

After confirming that diamond nanoneedle treatment does not cause measurable necrosis and DNA damage and the cell membrane integration at 3 h after treatment is also not affected, we then investigate whether the nanoneedle will lead to cell apoptosis and influence the intracellular G6PD level.

For cell apoptosis measurement, A549 cells were treated with a diamond nanoneedle array followed by culturing for 24 h. Subsequently, the cells were tested by Alexa fluor 488 annexin V/dead cell apoptosis kit. Annexin V was used as a probe to monitor apoptotic signals. In apoptosis, phosphatidylserine is exposed to the external cellular environment through lipid scrambling and annexin V can specifically bind to phosphatidylserine for detection of apoptosis of living cells. Red-fluorescent PI was used to stain cells in the early stage of necrosis by permeating the cell membranes and binding to nucleic acid within cells. Similar to the results shown in Figure 3, it can be seen from **Figure 4**a,b that diamond nanoneedle treatment alone does not induce notable cell death. Comparing to the control group (Figure 4a) (2.21%), the population of early necrotic cells in the groups of cells treated with a diamond nanoneedle array were low (1.57% in Figure 4b (cells were treated with a diamond nanoneedle array alone); 0.71% in Figure 4d (cells were treated with a diamond nanoneedle array and 5 μg mL^{-1} cisplatin). However, the total population of apoptotic A549 cells in the nanoneedle-treated group slightly increases from 1.31% to 3.17% (Figure 4a,b). Furthermore, when A549 cells are incubated with 5 μg mL^{-1} of cisplatin, the population of apoptotic A549 cells is 11.54%. When the cells are treated with nanoneedles and cisplatin at the same time, the population of apoptotic cells will increase to 16.59%. This also indicates the drug efficacy of cisplatin is enhanced through the aid of nanoneedle

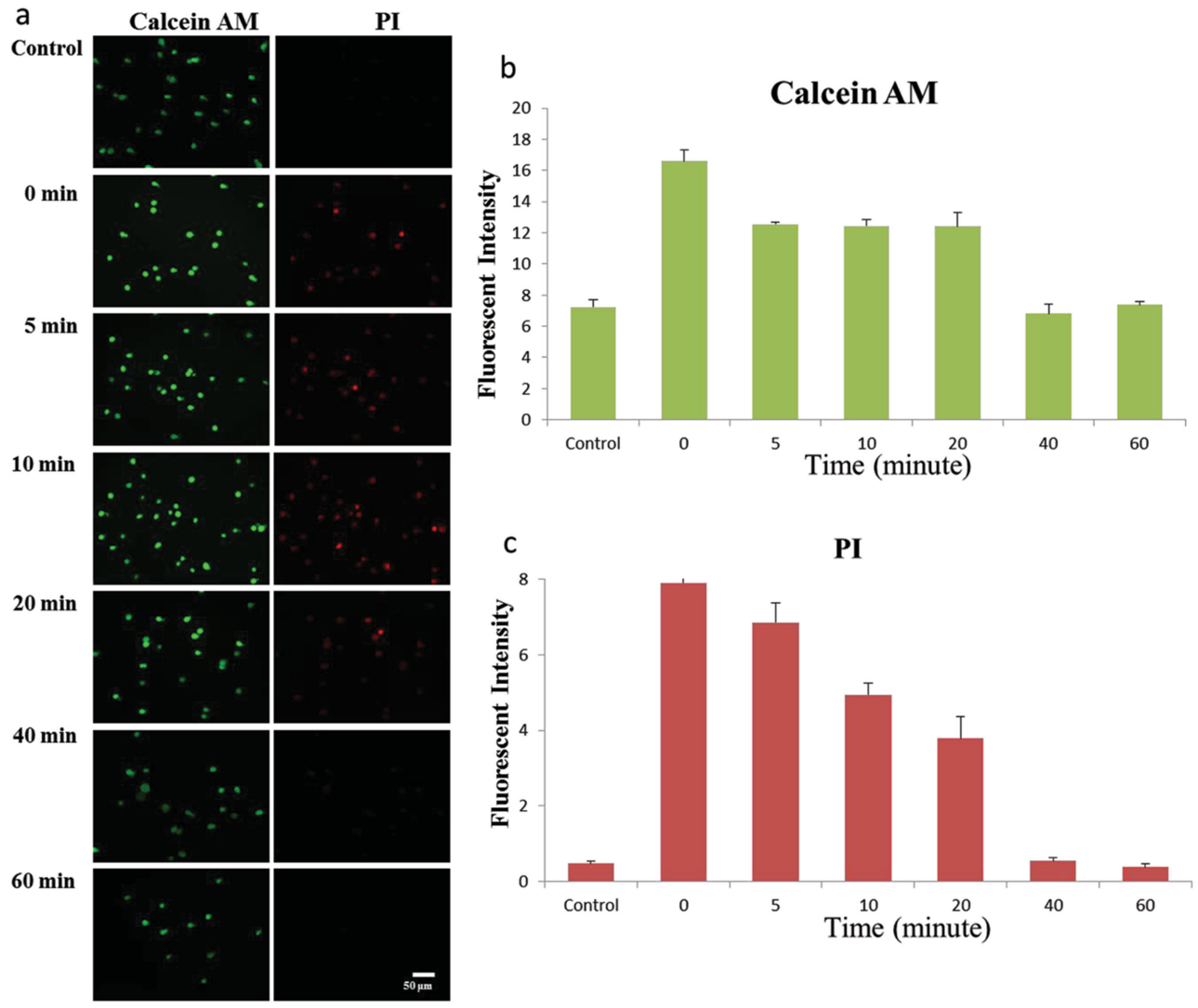

Figure 5. Cytosolic delivery of calcein-AM and PI in A549 cells. a) Calcein-AM (left) and PI (right) fluorescent images of living A549 cells when the chemicals were added at different time points after the cells being treated with nanoneedles. b) Quantification of calcein-AM fluorescent intensity of different groups. c) Quantification of PI fluorescent intensity at different time points. Untreated A549 cells were set as a control group.

treatment. In brief, the results show that nanoneedle treatment slightly induces cell apoptosis.

2.5. The Recovery of Mechanical Disruption on the Permeability of Cells

The enhanced intracellular delivery results (Figure 2), together with the apoptotic experiments (Figure 4) suggest the disruption on the cell membrane induced by nanoneedle treatment. In the meantime, the toxicity test (Figure 3) proves the integrity of the cytomembrane after diamond nanoneedle treatment. Therefore, it is useful to investigate the recovery process of the cell membrane after being treated with nanoneedles. This will also provide guidance on the application of the device.

For this purpose, calcein-AM and PI were chosen to stain the treated cells. Calcein-AM is highly lipophilic and cell membrane permeable dye, which can generate calcein from calcein-AM by esterase in a living cell and emit green fluorescence (maximum excitation: 490 nm, emission: 515 nm). Therefore, calcein-AM can only stain living cells. PI is not permeant to living cells, and therefore has been commonly used to detect the cells with comprised membranes such as dead cells. To understand the recovery of the cell membrane after nanoneedle disruption, calcein-AM and PI were added into the medium of the treated cells at different time points. The group without diamond nanoneedle treatment was set as a control group. In the control group, a certain number of calcein-AM molecules can enter the cells, but nearly no PI is able to diffuse to the cells because of the integrity of the cell membranes. Comparing with the control group, the cytosolic delivery of calcein-AM is dramatically enhanced when it was added immediately (0 min) after the cells being treated by nanoneedles (**Figure 5**a). This is within our expectation as the diamond nanoneedle treatment is supposed to improve the permeability of the cell membrane. With the increase of the

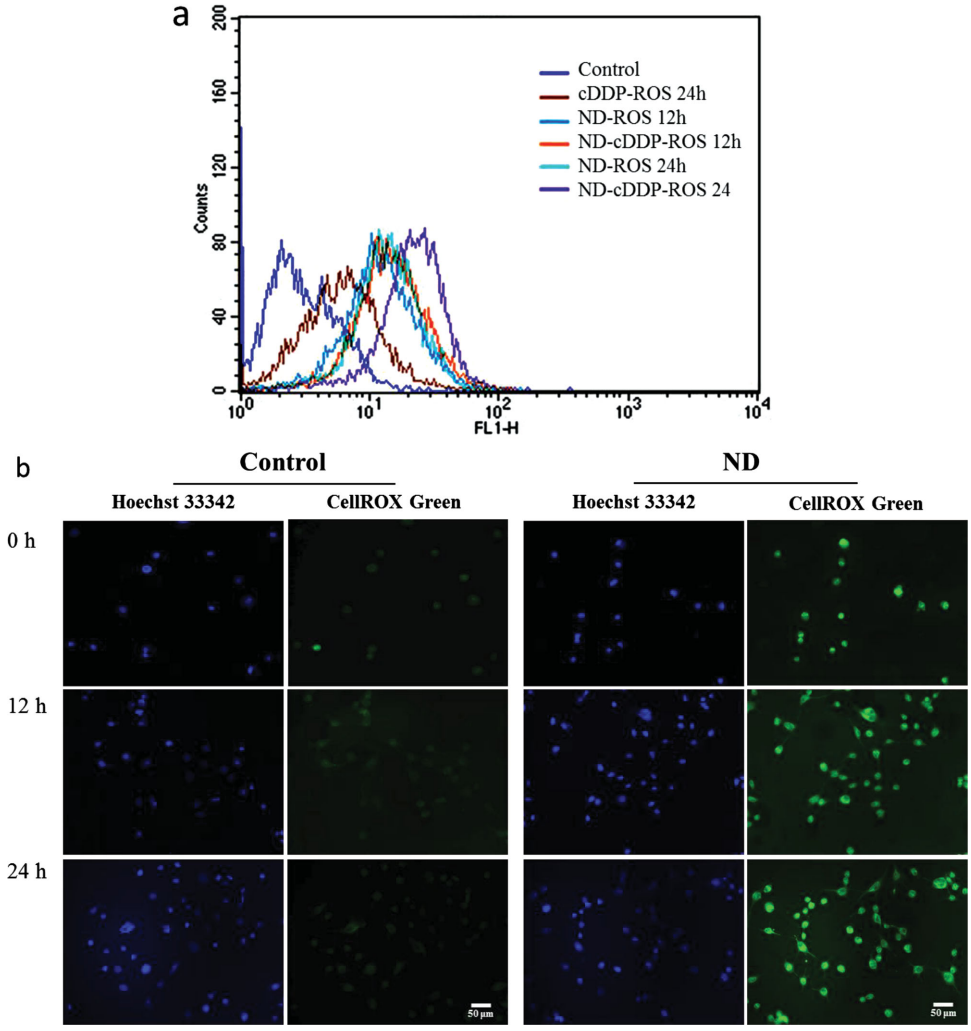

Figure 6. ROS content detection in A549 cells with nanoneedle array treatment. a) After incubating for 12 or 24 h, flow cytometry analysis was conducted to evaluate the ROS content in A549 cells. Cells treated with or without 1 μg mL^{-1} cisplatin (cDDP) addition and a nanoneedle array (ND) as indicated in the figure were stained with 5×10^{-6} M CellROX Green reagent (E_X/E_M 485/520 nm). b) Fluorescence images of ROS in A549 cells with or without nanoneedle array treatment (ND). Hoechst 33342 was used to stain cell nucleus. The cells without nanoneedle array treatment were used as control group. 0 h means immediately after nanoneedle treatment.

time, the cell membrane should gradually recover and therefore the permeation of molecules into the cells should slowly drop. After a certain period of time, the cell membrane is expected to completely recover, so the permeation of PI molecules into cells should not be possible any more. In line with this theory, we indeed find that the fluorescence intensity of the cells has the highest value at 0 min. When calcein AM was added at 5, 10, and 20 min after the cells being treated by nanoneedles, the fluorescence intensities slightly drop because fewer molecules are able to enter the cells. When calcein AM was added at 40 min or later, the fluorescence intensities fall to the level which is consistent with that of the control group (Figure 5a,b). This means that the cell membrane should have recovered its integrity. These findings are in fact fully supported by the PI staining result. For example, when PI was added to the medium at 40 min or later, negligible PI molecules can enter the cells, so the fluorescence can hardly be observed in the cells. We also calculate the percentages of PI positive cells at each time point. The results indicate that the percentage of PI positive cells are all above 90% within the 20 min period after nanoneedle treatment, but the value dramatically drops to a negligible amount (control level) at 40 min. Taking together, we suggest that diamond nanoneedle arrays penetration indeed disrupts cell membrane, but the integrity of the cell membrane can gradually recover within 40 min of nanoneedle treatment.

2.6. Nanoneedle Treatment Produces High Content of ROS

In order to examine the ROS content in cells, we used CellROX Green reagent. The dye is weakly fluorescent in a reduced state but displays high intensity of green fluorescence when oxidized by ROS. Untreated cells without staining were used as a negative control. The ROS content of cells was tested at two time points (12 and 24 h after treatment) under different conditions.

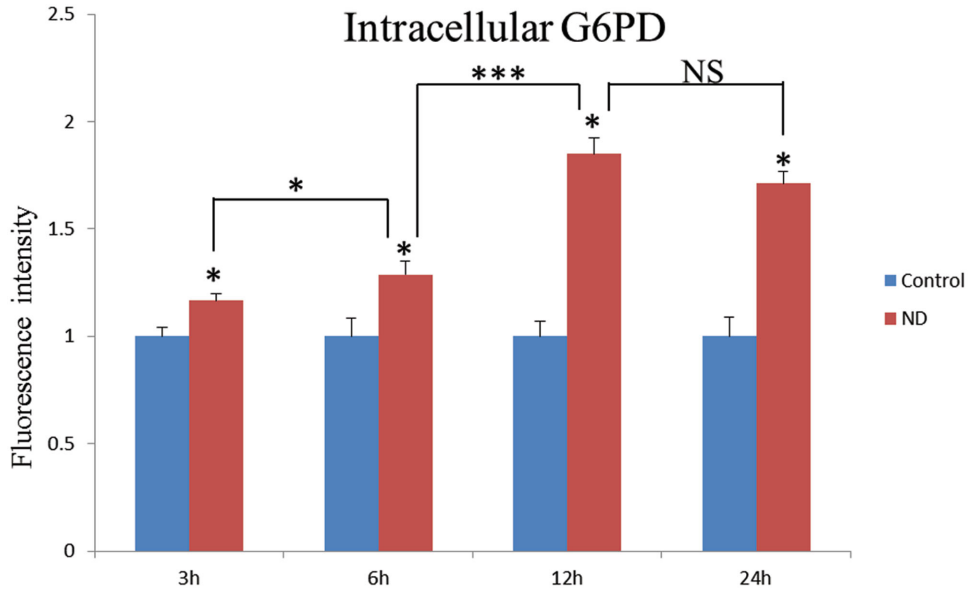

Figure 7. Intracellular G6PD activity assay. Untreated A549 cells were used as a control group. After being treated by a nanoneedle array platform (ND), A549 cells were cultured in a 96-well plate for 3, 6, 12, and 24 h as indicated. Then the cells were lysed and the activity of G6PD was measured in a microplate reader (E_X/E_M 530/590 nm). (*$P < 0.01$; NS: non-significant).

As shown in **Figure 6**a, after 24 h incubation, the relative fluorescent intensity of ROS in A549 cells treated with 1 μg mL^{-1} of cisplatin is 7.21. In contrast, the nanoneedle-treated cells had ROS levels of 14.03 and 15.18 at 12 and 24 h, respectively, after treatment. When cells were treated by nanoneedles and cisplatin, the ROS levels of A549 cells were elevated to 16.72 and 23.77 at 12 and 24 h, respectively, after treatment. From the fluorescence images shown in Figure 6b, we can see that, after 12 or 24 h incubation, nanoneedle array treatment could obviously elevate intracellular ROS production.

2.7. Nanoneedle Treatment Induces Increased Intracellular G6PD Level

The results in Figures 4 and 6 show that nanoneedle treatment leads to slightly increased apoptosis and higher ROS contents. When cells are jointly treated by nanoneedles and drug molecules (e.g., cisplatin), these findings may partially explain the reason of the improved drug efficacy when aided with nanoneedle treatment. However, according to our previous cytotoxicity measurement, the nanoneedle treatment alone will not lead to measurable cell death with MTT assay. We speculate that the elevated ROS level and apoptosis signal could trigger the redox components to counteract the negative effect of nanoneedle treatment to the physiology of the cells. The intracellular redox potential is determined by the ratio of oxidants and reductants. Nicotinamide adenine dinucleotide phosphate (NADPH) is the principal intracellular reductant that can be used by many enzymes for reducing power in cells such as glutathione reductase and catalase.[28] G6PD is the first and rate-limiting enzyme of pentose phosphate (PP) signal pathway to determine the NADPH production by controlling the metabolism of glucose via PP signal pathway.[29] G6PD and NADPH have an essential role to counterbalance the oxidative stress and protect cells from oxidative stress-induced apoptosis.[30–32] To monitor the intracellular G6PD levels, A549 cells were treated with a diamond nanoneedle array and the measurement was performed at 3, 6, 12, and 24 h after the treatment. For untreated cells, the test was also carried out at all different time points for comparison. As shown in **Figure 7**, compared with the control groups, the intracellular G6PD level in A549 cells is dramatically increased with time increasing and reaches the highest level at 12 h and slowly drops to normal level after 48 h culture. (Figure S5, Supporting Information). However, combining with the result shown in Figure 4, we speculate that the increased G6PD activity still could not completely balance the high ROS content, and therefore the treatment still led to slight elevation of apoptosis signal pathway.

2.8. Depolarization of Mitochondrial Membrane Potential

After knowing that the diamond nanoneedle array treatment can cause the production of ROS, we next studied the possible reasons. Mitochondria is an important organelle that plays a central role in cellular viability, such as heat generation, cell growth, cell death via apoptosis, passive proton leak, formation, and degradation of ROS.[33–37] Via different experimental models, it has been repeatedly demonstrated that a lower mitochondrial membrane potential is observed with a simultaneously increase of ROS production.[38,39] In this study, we used the MitoProbe JC-1 assay kit to test mitochondrial membrane potential. JC-1 is a lipophilic dye and can selectively enter into mitochondria with a reversible change of color from green (529 nm) to red (590 nm) as the membrane potential increases. The mitochondrial membrane potential was detected at three different time points (0, 12, and 24 h). At first, the ratio of red/green (R3/R2) decreases immediately after the nanoneedle arrays treatment. But after 12 h, or

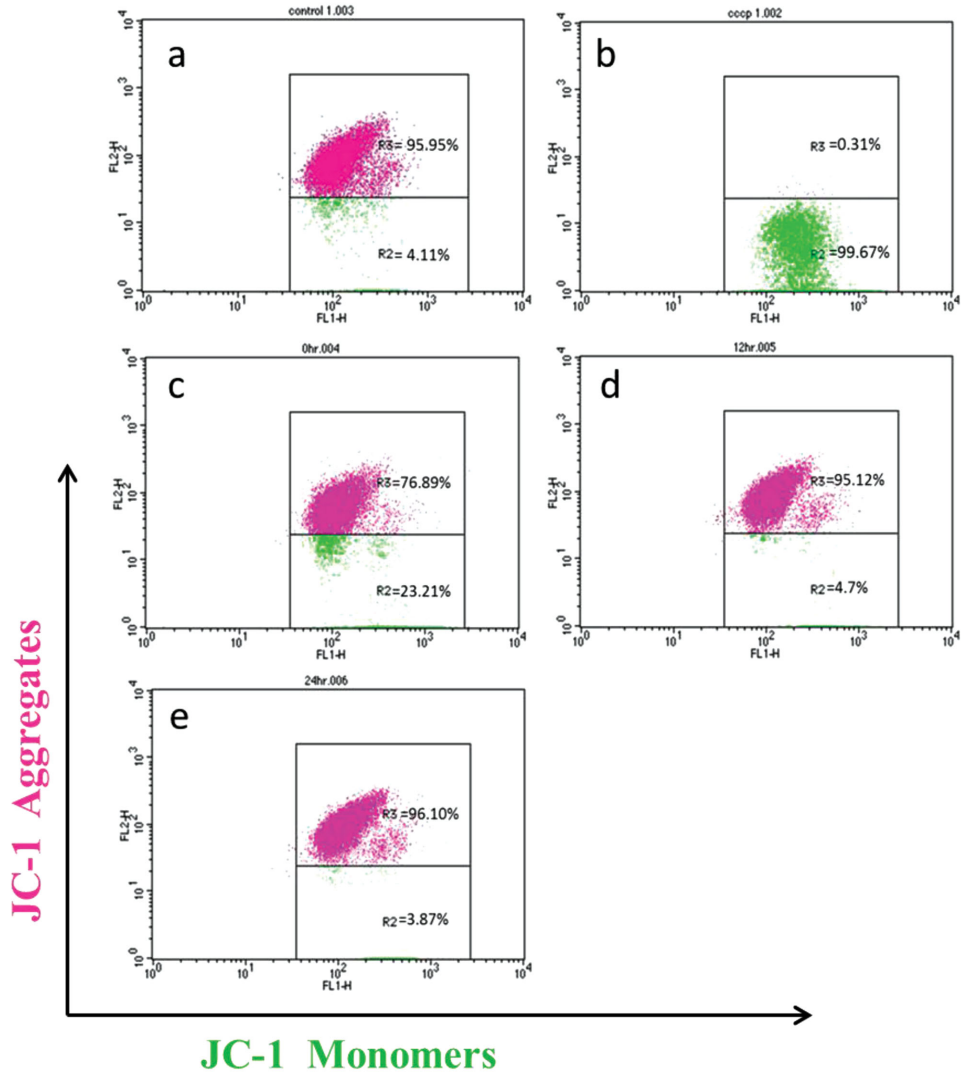

Figure 8. Flow cytometry assay of mitochondrial membrane potential. a) Untreated A549 cells were used as positive control. b) Untreated A549 cells with 50×10^{-6} M cccp (carbonyl cyanide 3-chlorophenylhydrazone) were used as a negative control. Following the nanoneedle array treatment, A549 cells were stained with 2×10^{-6} M JC-1 immediately c), or after d) 12 or e) 24 h incubation. Cells were analyzed on flow cytometer using 488 nm excitation with 530/30 nm and 585/42 nm band-pass emission filters. The intensity of green and red fluorescence intensities is shown as R2 and R3, respectively.

longer (24 h), the mitochondrial membrane potential recovers to normal ratio when compared with control group (**Figure 8**). This indicates that the depolarization of mitochondrial membrane potential could be one of the reasons of the generation of ROS. However, some production of non-mitochondrial ROS could not be completely excluded, such as the membrane-bound NADPH oxidase.[40] Further experiments will be necessary to understand the generation of ROS and its influence on the cell physiology.

3. Conclusion

In summary, our results show that centrifugation force regulated diamond nanoneedle treatment of cell suspensions could deliver molecules into cells in an efficient way. Attractively, the approach does not induce noticeable cytotoxicity indicated by the viability of nanoneedle-array-treated cells and genotoxicity suggested by the lack of pH2AX expression. However, the treatment leads to increased ROS content and cell apoptosis. The elevated annexin V binding to the cell membranes, shown by the increased apoptosis of cells, reveals that diamond nanoneedle array disruption can induce lipid scrambling and then affect the intracellular metabolic signal pathways. For the cells only treated by our nanoneedle arrays, these do not induce much cytotoxicity. The reason might be that their damaging to the cells is partially counteracted by the elevation of G6PD. It is possible that the production of ROS content during nanoneedle array treatment is partially caused by the decreased mitochondrial membrane potential (**Figure 9**). Importantly, by using calcein-AM and PI double staining, we explored that the cell

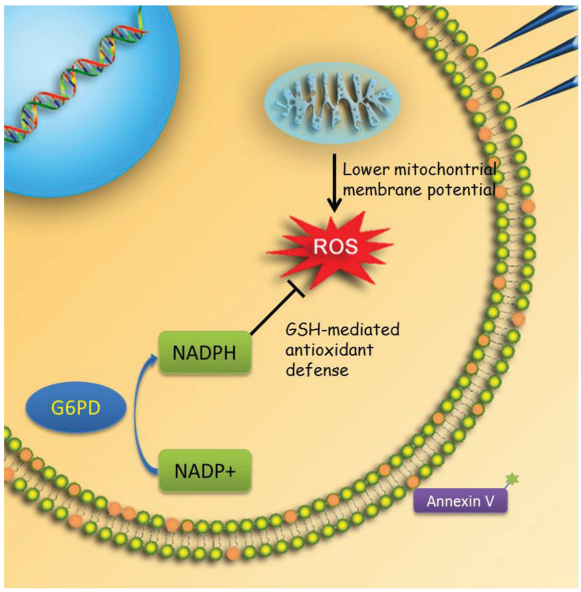

Figure 9. Schematic representation of the influence of diamond nanoneedle array treatment on the intracellular metabolic system. Following the diamond nanoneedle arrays penetration, the phosphatidylserine is exposed to the extracellular environment and can bind with annexin V. The nanoneedle treatment leads to a significant decrease of mitochondrial membrane potential. As a result, a high content of ROS is produced under the increased oxidant stress. Under this oxidant environment, the activity of intracellular redox enzymes G6PD is aroused to counterbalance the high production of ROS. In the process, NADPH is synthesized and utilized by the glutathione (GSH)-mediated antioxidant defense.

membranes should fully recover within 40 min after diamond nanoneedle treatment.

In summary, this is the first report in which we systematically investigated the influence of diamond nanoneedle array treatment on the metabolic signal pathways of cells. It could provide a new arena for exploiting the nanoneedle application.

4. Experimental Section

Fabrication of Diamond Nanoneedle Arrays: Diamond nanoneedle arrays were produced by a top-down method. First, polycrystalline diamond thin film was fabricated by microwave plasma chemical vapor deposition (MPCVD). N-type silicon wafer (100)–oriented, 1–10 Ω, was polished with diamond particle paste (0.25 μm) was used as a substrate. Silicon substrate was then put into ultrasonic bath with alcohol and acetone for cleaning.

The ASTeX MWCVD reactor connected with a 1.5 kW microwave generator was accounted for deposition of polycrystalline diamond film. Methane (CH_4) and hydrogen (H_2) in the ratio 1% and 99% were being used as gas precursor, with the total flow rate of 300 SCCM. The temperature, pressure, and microwave power were maintained at 800 °C, 30 Torr, and 1200 W, respectively, for 24 h. Second, after synthesis of diamond film, it was etched to diamond nanocone arrays by using electron cyclotron resonance microwave plasma chemical vapor deposition (ECR-MPCVD). Around 875G B-field were generated by an external magnetic coil to the center of the chamber. Gases mixture of 70% He, 25% Ar, 5% N_2 were used to induce plasma by 1400 W microwave source. The temperature and pressure were kept at 400 °C and 2×10^{-3} Torr, respectively.

Cell Cultures: A549 cells (ATCC) were maintained in Dulbecco's modified eagle medium (DMEM, Life Technology) supplemented with 10% fetal bovine serum hyclone, L-glutamine and 1% penicillin/streptomycin at 37 °C with 5% CO_2. Doxorubicin resistant MCF7 cell line (DR-MCF7) was cultured in full medium with the addition of 2 μg mL^{-1} doxorubicin (Sigma) for achieving doxorubicin resistance.

Diamond Nanoneedle Arrays to Facilitate Intracellular Delivery: Adherent cells were first trypsinized to obtain a cell suspension. Then the cell suspension was placed onto a diamond nanoneedle array located in a 24-well cell culture plate (2×10^4 cells per well) followed by centrifugation at 120 g for 5 min at room temperature (CT15RT Eppendorf, Germany). This is the standard nanoneedle treatment condition in this paper unless otherwise specified. The experiments were performed in three groups for each cargo material of cisplatin and dextran–FITC. The first and second groups contained cargo molecules of cisplatin (or dextran–FITC), but only one group of cells experienced diamond nanoneedle treatment. The third group did not have any cargo molecules and acted as an untreated negative control. In this paper, untreated control group means that the cells were not treated with centrifugation. After centrifugation, the cell suspension was removed from the diamond nanoneedle arrays and then harvested for subsequent operations.

Cytotoxicity Assay: The releasing level of glucose 6-phosphate (G6PD) was measured by the G6PD release assay kit (Invitrogen, USA). Briefly, after nanoneedle treatment, cells were transferred to a 96-well plate and cultured for 6 h in a volume of 50 μL. Then 50 μL of resazurin was added into the plate to a concentration 15×10^{-6} M. After 10–30 min incubation at 37 °C, the fluorescence intensity was read by a fluorescence microplate reader (BMG Polarstar Optima, Ortenberg, Germany) with appropriate excitation (530–560 nm) and emission filters (580–600 nm).

Cell viability was tested by MTT assay. After nanoneedle treatment, cells were transferred into a 96-well plate and cultured for 48 h at 37 °C. Then the medium was removed and replaced with 100 μL of fresh culture medium containing no cargo molecules. 10 μL of 12×10^{-3} M MTT stock solution was added into each well followed by incubation at 37 °C for 4 h. Subsequently, all media were removed and replaced with 100 μL DMSO. Finally, the absorbance at 540 nm of each sample was measured by a UV–Vis–IR microplate reader (Powerwave XS MQX200R, Leicestershire, England).

Flow Cytometry: The apoptosis assay was conducted according the protocol of Alexa Fluor 488 annexin V/dead cell apoptosis kit (Invitrogen, Carlsbad, USA). A 488 nm laser served as an exciting source for annexin V-FITC (FL1, 530/30 nm) and PI (FL2, 575/24 nm) (BD FACSCalibur, flow cytometer).

For studying the delivery of doxorubicin into MCF/ADR cells, three groups were conducted. The first group of MCF7/ADR cells was incubated with 2 μg mL^{-1} doxorubicin for 5 min without diamond nanoneedle treatment. The second group was treated by diamond nanoneedle arrays for 5 min with the addition of 2 μg mL^{-1} doxorubicin. Untreated MCF7/ADR cells were used as control. Then three groups of cell suspension were collected and washed by PBS for two times to remove the extra doxorubicin and resuspended in PBS for flow cytometry analysis with excitation at 488 nm and emission filter at 580 nm.

ROS was measured by the CellROX Green Reagent (Invitrogen, Carlsbad, USA) in living cells. CellROX green reagent was added into a medium to a final concentration of 5×10^{-6} M and incubated with cells for 30 min at 37 °C. Then cells were washed for three times with PBS for flow cytometry studying (E_X/E_M 488/520 nm).

Fluorescent Microscopy: After centrifugation, cells delivered with dextran fluorescent 488 (10 000 MW, Invitrogen, Carlsbad USA) were incubated with 2 μL of 20×10^{-3} M Hoechst33342 (Invitrogen, Carlsbad, USA) for 20 min for nuclei staining at 37 °C. Cellular fluorescence was monitored using fluorescence microscopy.

pH2AX Detection and Image-iT Dead Green Staining: The level of pH2AX was measured by HCS DNA damage kit (Invitrogen, Carlsbad, USA) with the following procedures. First, after being treated by a diamond nanoneedle array, cells were transferred to a 96-well plate and

cultured for 3, 6, or 24 h. Second, the cells were stained with image-iT Dead Green viability stain working solution for 30 min at 37 °C. Third, the cells were fixed with 4% paraformaldehyde solution for 15 min, washed with PBS, and incubated with a permeabilization solution of 15 µL of Triton X-100 to 6 mL PBS at room temperature. Fourth, the samples were washed with PBS and incubated with blocking buffer containing 1% BSA for 60 min. Fifth, the samples were incubated with the primary pH2AX antibody for 60 min and washed with PBS for three times. Sixth, the secondary antibody Alexa Fluor 555 goat anti-mouse IgG (H+L) was added and incubated for another 60 min. Seventh, the secondary antibody was removed and the cells were rinsed with PBS. Eighth, 100 µL of fresh PBS was added into each well for analysis. The samples were scanned by microplate reader (BMG Polarstar Optima, Ortenberg, Germany) with filters appropriate for Hoechst (350/461 nm), Image-iT Dead Green viability stain (488/515 nm) and Alexa Fluor 555 goat anti-mouse IgG (555/565 nm).

Calcein-AM and PI Staining: After being treated by the diamond nanoneedle arrays, A549 cells were suspended in PBS. Calcein-AM and PI were added into the cell suspensions at different time points and incubated at 37 °C for 20 min. Then the cells were washed by PBS for two times and the cellular fluorescence was monitored by fluorescence microscopy and analyzed with ImageJ. A549 cells without nanoneedle treatment were set as a control group.

Statistical Analysis: Experiments were repeated at least three times. For each set of the experiments, results were expressed as mean values ± standard deviation. Statistical significance was calculated by either the student *t*-test for paired comparisons or the one-way ANOVA for multiple comparisons. A p value <0.05 was considered as significance.

Supporting Information

Supporting Information is available from the Wiley Online Library or from the author.

Received: December 6, 2015
Revised: February 8, 2016
Published online: March 15, 2016

[1] B. Leader, Q. J. Baca, D. E. Golan, *Nat. Rev. Drug Discovery* **2008**, *7*, 21.
[2] R. Kole, A. R. Krainer, S. Altman, *Nat. Rev. Drug Discovery* **2012**, *11*, 125.
[3] W. Kim, J. K. Ng, M. E. Kunitake, B. R. Conklin, P. D. Yang, *J. Am. Chem. Soc.* **2007**, *129*, 7228.
[4] J. Yu, X. Diao, X. Zhang, X. Chen, X. Hao, W. Li, X. Zhang, C. S. Lee, *Small* **2014**, *10*, 1125.
[5] J. Yu, X. J. Zhang, X. J. Hao, X. H. Zhang, M. J. Zhou, C. S. Lee, X. F. Chen, *Biomaterials* **2014**, *35*, 3356.
[6] S. Zhou, X. Du, F. Cui, X. Zhang, *Small* **2014**, *10*, 980.
[7] L. Yan, J. Zhang, C. S. Lee, X. Chen, *Small* **2014**, *10*, 4487.
[8] A. J. Phillips, *J. Pharm. Pharmacol.* **2001**, *53*, 1169.
[9] Y. Liu, H. Wang, K. Kamei, M. Yan, K. J. Chen, Q. H. Yuan, L. Q. Shi, Y. F. Lu, H. R. Tseng, *Angew. Chem. Int. Ed.* **2011**, *50*, 3058.
[10] R. Kanasty, J. R. Dorkin, A. Vegas, D. Anderson, *Nat. Mater.* **2013**, *12*, 967.
[11] M. Oba, M. Tanaka, *Biol. Pharm. Bull.* **2012**, *35*, 1064.
[12] T. K. Kim, J. H. Eberwine, *Anal. Bioanal. Chem.* **2010**, *397*, 3173.
[13] M. S. Al-Dosari, X. Gao, *AAPS. J.* **2009**, *11*, 671.
[14] L. Yan, Y. Yang, W. J. Zhang, X. F. Chen, *Adv. Mater.* **2014**, *26*, 5533.
[15] A. K. Shalek, J. T. Robinson, E. S. Karp, J. S. Lee, D. R. Ahn, M. H. Yoon, A. Sutton, M. Jorgolli, R. S. Gertner, T. S. Gujral, G. MacBeath, E. G. Yang, H. P. Park, *Proc. Natl. Acad. Sci. USA* **2010**, *107*, 1870.
[16] J. J. VanDersarl, A. M. Xu, N. A. Melosh, *Nano Lett.* **2012**, *12*, 3881.
[17] S. J. Qi, C. Q. Yi, S. L. Ji, C. C. Fong, M. S. Yang, *ACS Appl. Mater. Interfaces* **2009**, *1*, 30.
[18] H. Persson, C. Kobler, K. Molhave, L. Samuelson, J. O. Tegenfeldt, S. Oredsson, C. N. Prinz, *Small* **2013**, *9*, 4006.
[19] D. D. Liu, C. Q. Yi, K. Q. Wang, C. C. Fong, Z. K. Wang, P. K. Lo, D. Sun, M. S. Yang, *ACS Appl. Mater. Interfaces* **2013**, *5*, 13295.
[20] E. Y. W. Chong, C. Y. P. Ng, V. W. Y. Choi, L. Yan, Y. Yang, W. J. Zhang, K. W. K. Yeung, X. F. Chen, K. N. Yu, *J. Mater. Chem. B* **2013**, *1*, 3390.
[21] Y. Wang, Y. Yang, L. Yan, S. Y. Kwok, W. Li, Z. Wang, X. Zhu, G. Zhu, W. Zhang, X. Chen, P. Shi, *Nat. Commun.* **2014**, *5*, 4466.
[22] X. F. Chen, G. Y. Zhu, Y. Yang, B. L. Wang, L. Yan, K. Y. Zhang, K. K. W. Lo, W. J. Zhang, *Adv. Healthcare Mater.* **2013**, *2*, 1103.
[23] L. Yan, A. P. Raphael, X. Y. Zhu, B. L. Wang, W. Chen, T. Tang, Y. Deng, H. J. Sant, G. Y. Zhu, K. W. Choy, B. K. Gale, T. W. Prow, X. F. Chen, *Adv. Healthcare Mater.* **2014**, *3*, 555.
[24] M. Choi, S. H. Lee, W. B. Kim, V. Gujrati, D. Kim, J. Lee, J. I. Kim, H. Kim, P. E. Saw, S. Jon, *Adv. Healthcare Mater.* **2015**, *5*, 101.
[25] C. Chiappini, E. De Rosa, J. O. Martinez, X. Liu, J. Steele, M. M. Stevens, E. Tasciotti, *Nat. Mater.* **2015**, *14*, 532.
[26] B. Jakob, J. Splinter, S. Conrad, K. O. Voss, D. Zink, M. Durante, M. Lobrich, G. Taucher-Scholz, *Nucleic Acids Res.* **2011**, *39*, 6489.
[27] P. Karran, *Curr. Opin. Genet. Dev.* **2000**, *10*, 144.
[28] Z. Y. Zhang, C. W. Liew, D. E. Handy, Y. Y. Zhang, J. A. Leopold, J. Hu, L. L. Guo, R. N. Kulkarni, J. Loscalzo, R. C. Stanton, *FASEB J.* **2010**, *24*, 1497.
[29] R. F. Kletzien, P. K. W. Harris, L. A. Foellmi, *FASEB J.* **1994**, *8*, 174.
[30] E. Akkemik, H. Budak, M. Ciftci, *J. Enzyme Inhib. Med. Chem.* **2010**, *25*, 476.
[31] P. Arese, V. Gallo, A. Pantaleo, F. Turrini, *Transfus. Med. Hemother.* **2012**, *39*, 328.
[32] M. D. Cappellini, G. Fiorelli, *Lancet* **2008**, *371*, 64.
[33] R. Acin-Perez, D. L. Gatti, Y. D. Bai, G. Manfredi, *Cell Metab.* **2011**, *13*, 712.
[34] M. P. Murphy, *Biochem. J.* **2009**, *417*, 1.
[35] D. W. Kamp, E. Shacter, S. A. Weitzman, *Oncology* **2011**, *25*, 400.
[36] M. Huttemann, P. Pecina, M. Rainbolt, T. H. Sanderson, V. E. Kagan, L. Samavati, J. W. Doan, I. Lee, *Mitochondrion* **2011**, *11*, 369.
[37] V. Geromel, N. Kadhom, I. Cebalos-Picot, O. Ouari, A. Polidori, A. Munnich, A. Rotig, P. Rustin, *Hum. Mol. Genet.* **2001**, *10*, 1221.
[38] M. P. Murphy, A. Holmgren, N. G. Larsson, B. Halliwell, C. J. Chang, B. Kalyanaraman, S. G. Rhee, P. J. Thornalley, L. Partridge, D. Gems, T. Nystrom, V. Belousov, P. T. Schumacker, C. C. Winterbourn, *Cell Metab.* **2011**, *13*, 361.
[39] X. J. Wu, T. Stahl, Y. Hu, F. Kassie, V. Mersch-Sundermann, *J. Nutr.* **2006**, *136*, 608.
[40] H. Mizutani, S. Tada-Oikawa, Y. Hiraku, M. Kojima, S. Kawanishi, *Life Sci.* **2005**, *76*, 1439.